Review Article

# MR imaging of the traumatic triangular fibrocartilaginous complex tear

**Alex W. H. Ng[1], James F. Griffith[1], Cindy S. Y. Fung[2], Ryan K. L. Lee[1], Cina S. L. Tong[1], Clara W. Y. Wong[3], Wing Lim Tse[3], Pak Cheong Ho[3]**

[1]Department of Imaging and Interventional Radiology, Prince of Wales Hospital, The Chinese University of Hong Kong, Hong Kong, China; [2]Department of Diagnostic Imaging, North District Hospital, Hong Kong, China; [3]Department of Orthopedics and Traumatology, Prince of Wales Hospital, The Chinese University of Hong Kong, Hong Kong, China

*Correspondence to:* Dr. Alex W. H. Ng, MBChB, FRCR. Department of Imaging and Interventional Radiology, Prince of Wales Hospital, 30-32 Ngan Shing Street, Shatin, N.T. Hong Kong, China. Email: alex@sunghim.com.

**Abstract:** Triangular fibrocartilage complex is a major stabilizer of the distal radioulnar joint (DRUJ). However, triangular fibrocartilage complex (TFCC) tear is difficult to be diagnosed on MRI for its intrinsic small and thin structure with complex anatomy. The purpose of this article is to review the anatomy of TFCC, state of art MRI imaging technique, normal appearance and features of tear on MRI according to the Palmar's classification. Atypical tear and limitations of MRI in diagnosis of TFCC tear are also discussed.

**Keywords:** MRI; arthrogram; wrist; the triangular fibrocartilage complex (TFCC); tear

Submitted Jul 01, 2017. Accepted for publication Jul 14, 2017.
doi: 10.21037/qims.2017.07.01
**View this article at:** http://dx.doi.org/10.21037/qims.2017.07.01

## Clinical relevance

The triangular fibrocartilage complex (TFCC) serves to stabilize the distal radioulnar joint (DRUJ) by acting as cushion for the ulnar head and lunate during the axial loading of the wrist and ulnar deviation of the wrist (1-3). It also limits ulnar deviation of the carpus (4).

TFCC tear often results from a fall onto outstretched hand which severely increases axial loading or a hyperpronation injury to the forearm (5). TFCC tear usually presents as ulnar-sided wrist pain.

Another clinical manifestation of TFCC injury is DRUJ instability. DRUJ instability can result in audible clicking and pain during rotation of the forearm (6). Usually patients have dorsal subluxation of the ulnar head on extreme hyperpronation due to disruption of the dorsal radioulnar ligament of the TFCC and dorsal DRUJ capsule (4).

Chronic TFCC tear can result in premature degeneration of the ulnocarpal joint or DRUJ with osteophytosis, cartilage loss, subchondral sclerosis, subchondral oedema and cystic change. Chronic ulnar-sided wrist pain and swelling with synovitis usually ensures.

## Normal anatomy

The TFCC is composed of ligament, cartilage and tendon. These include the triangular fibrocartilagous articular disc, volar and dorsal radioulnar ligaments, volar ulnotriquetral and ulnolunate ligaments, ulnar collateral ligament, extensor carpi ulnaris (ECU) tendon sheath and ulnomeniscal homologue (3,7-9).

The central component of the TFCC is a triangular fibrocartilage (*Figure 1*). The ulnar side is broader while the dorsal and volar sides are thicker, giving it a bowtie appearance on sagittal view. It may be fenestrated centrally, especially in elderly due to degeneration. Ulnar positive variant patients have thinner articular discs while the reverse is true for ulnar negative patients making them more or less prone to tendon degeneration and tears respectively (10).

On the volar side, the triangular fibrocartilage merges completely with the volar radioulnar ligament which is reinforced by the ulnotriquetral and ulnolunate ligaments (*Figure 1*). These insert onto the volar aspect of the lunate and triquetrum respectively, forming the anterior band of the triquetral sling (11).

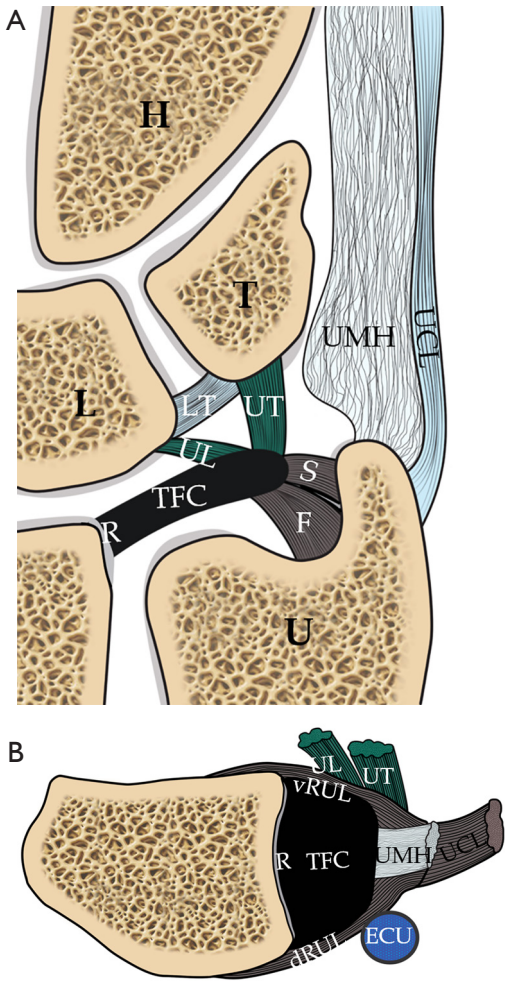


**Figure 1** Schematic diagram shows all the TFCC components, including coronal (A) and axial (B) images. The triangular fibrocartilage or articular disc is a central component of the TFCC. On the medial side, the TFC attaches to ulnar styloid process by a distal lamina (S) and the ulnar fovea by a proximal lamina (F). On the dorsal and volar aspects, the TFC is inseparable from the dRUL and vRUL. On the radial side, the TFC attaches to the distal radial articular cartilage (R). Towards the dorsal side of the ulnar aspect, the TFC attaches to the UMH and the UCL. At around this region, the TFC also attaches to the ECU tendon sheath. On the volar aspect, the TFC attaches to the lunate (L) and triquetral (T) bones via the ulnotriquetral (UT) and ulnolunate (UL) ligaments respectively. U, distal ulna; H, hamate. TFCC, triangular fibrocartilage complex; dRUL, dorsal radioulnar ligament; vRUL, volar radioulnar ligaments; UMH, ulnomeniscal homologue; UCL, ulnar collateral ligament; ECU, extensor carpi ulnaris.

On the dorsal side, the triangular fibrocartilage merges with the dorsal radioulnar ligament which is reinforced by the dorsal radiotriquetral ligament (dorsal radiocarpal ligament) forming the posterior band of the triquetral sling (*Figure 1*). Since the volar and dorsal radioulnar ligament are so closely integrated with the articular disc, some authors consider this as simply thick, strong marginal portions of the disc composed of lamellar collagen (4).

At the ulnar side, the triangular fibrocartilage is attached to the inner side of the ulnar styloid process (just proximal to the ulnar tip) by a distal lamina and ulnar fovea by a proximal lamina (*Figure 1*). The disc is broader at this region. The tissue in between the two laminae is loose, though highly vascularized, areolar tissue named the ligamentum subcruentum.

At the ulno-dorsal aspect of the TFCC, the triangular fibrocartilage is reinforced by meniscal homologue which is situated in between the ulna and triquetrum (*Figure 1*). It has a common origin with the dorsal radioulnar ligament on the ulno-dorsal corner of the radius (12) and inserts on the ulnar border of triquetrum and 5$^{th}$ metacarpal base.

Some of TFCC fibres are also reinforced by ECU tendon sheath (13). The ECU is situated within the ulnar notch and surrounded by its synovial sheath and the investing fascia of the wrist (4). They are further reinforced by the ulnar collateral ligament which blends with the ECU tendon sheath. It is noteworthy that there is no prominent ulnar collateral ligament demonstrable on MR imaging (4,14) and the existence of this as an isolated structure has been challenged (15).

On the radial side, the triangular fibrocartilage is attached to the articular cartilage covering the ulnar side of the distal radius (*Figure 1*).

The ulnar side of the articular disc and its supporting structures are supplied by the ulnar and anterior interosseous arteries (16). The central and radial aspects of the disc are relatively avascular and comprise of chondrocytes in a fibrocartilaginous matrix, helping to explain why central and radial tear of the triangular fibrocartilage do not heal well if repaired (17).

## MRI technique

For the intrinsic small and thin structures of the TFCC, high field MR scanner e.g., 3 Tesla MR scanner is ideally used to acquire a high spatial, high contrast imaging data (1,18).

The 'superman position' with the hand raised up and above the head can allow the wrist to be scanned

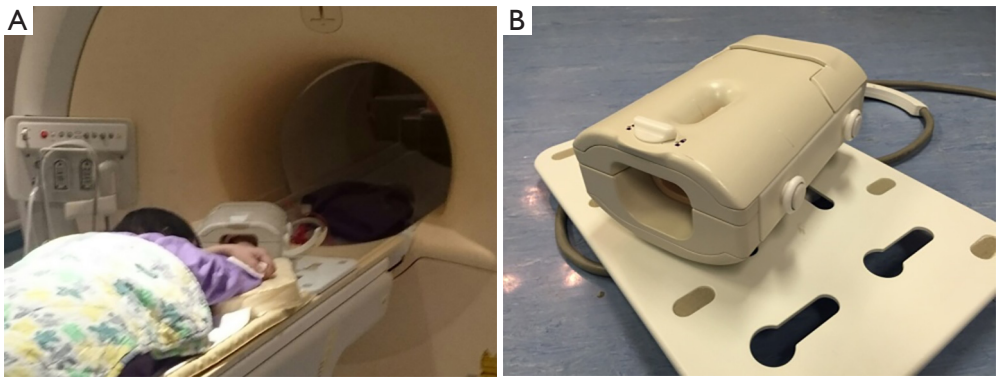


**Figure 2** Real time situation when the patient is undergoing MRI examination of the wrist within the MRI scanner. (A) In the MRI scanner, the patient lies prone with the hand above the head in a "superman" position. Superman position allows the wrist to be scanned in the isocenter of the magnetic field, which is more homogeneous. The wrist in this position is slightly semipronated; (B) a dedicated wrist coil achieves a high resolution and signal to noise ratio. Motion artefact is the most commonly encountered problem during wrist imaging as the patient needs to maintain still for approximately 20–30 minutes in prone and superman position.

in the isocenter of the magnetic field, which is more homogeneous. The wrist in this position will be slightly semipronated (*Figure 2A*). The wrist should ideally be scanned in a dedicated eight-channel wrist coil (*Figure 2B*) which will enable acquisition of high resolution imaging data to more clearly depict the small structures of the TFCC.

Multiple different pulse sequences can be used for imaging the TFCC including spin echo and fat-suppression sequences (1). In our centre, we use high resolution proton density coronal with fat and non-fat suppression sequences, sagittal T2W fat-suppression sequence and axial proton-density fat suppression sequences. Three orthogonal planes are acquired allowing good correlation with each other.

Proton density sequences with or without fat suppression can detect intradiscal degeneration. A tear is seen as fluid signal filling an abnormal anatomical gap on T2W fat suppressed sequences.

3D gradient echo sequences allow the acquisition of thin contiguous sections 1mm or less through the TFCC (19) and no interslice gap. A recent study showed that punctate calcifications within the disc indicating degeneration were best depicted on the 3D gradient echoes sequence (20). Quantitative MRI such as T1 rho to look for changes of mechanical properties of TFCC is still under research.

Although the sensitivity and specificity of MR arthrography is overall unquestionably slightly better than non-arthrographic MR imaging, in most instances it is not necessary to perform an MR arthrogram to adequately assess the structures of the TFCC. Whether or not to undertake MR arthrography should consider local expertise, time and cost efficiency, patient comfort, and clinical need. The vast majority of surgically relevant pathology will be visible on a non-arthrographic MR study, especially nowadays with higher resolution data acquisition. Minor perforations and small tears may be missed on non-arthrographic studies though the relevance of these relatively minor injuries with respect to surgical decision making is highly questionable in most patients (3). In our institution, we perform MR arthrography for younger patients, particularly if they are athletic and/or considered good surgical candidates, or if they have unexplained ulnar wrist symptoms with a prior relatively normal non-arthrographic MR study of the wrist. MR arthrography risks contamination of soft tissue detail by contrast extravasation, does not allow one to appreciate joint effusion and seems to lessen the depiction of mild ulnocarpal synovitis.

MR arthrography can be indirect or direct (21-22). Direct arthrography is performed using ultrasound or fluoroscopic guidance (23) (*Figure 3*). We prefer to use ultrasound approach primarily for its superior real time capability. Though a limitation can be leakage of contrast from one wrist compartment to the other due to a communicating tear which cannot be seen during the injection.

Both ultrasound and flurosocopic guidance are from the dorsal side because it is more superficial with less intervening crucial anatomical structures.

Usually contrast injected into the radiocarpal joint is enough to delineate any communicating tear. Contrast will fill the gap of the tear allowing clear depiction by MRI. If

 

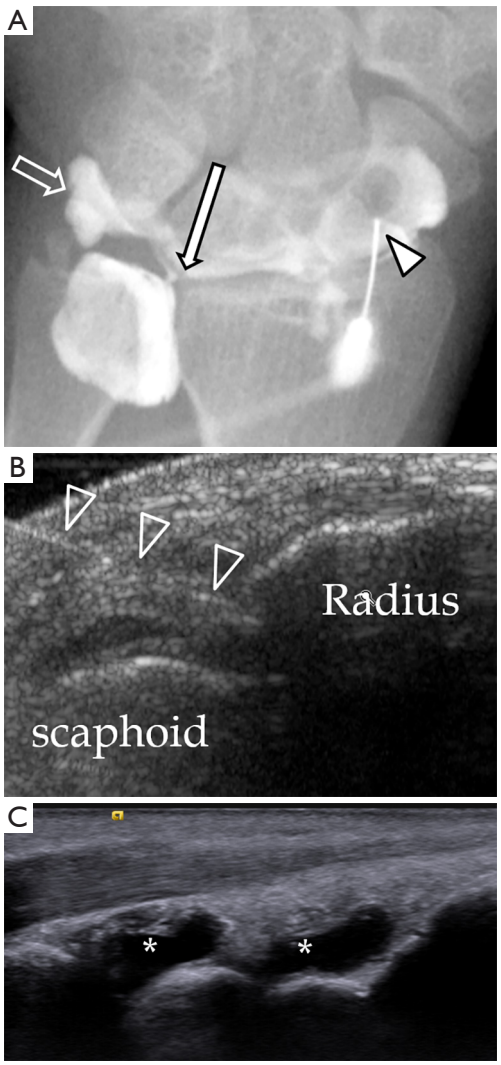


**Figure 3** Injection of diluted gadolinium is needed to obtain a good MR arthrogram. (A) Fluoroscopic guidance is the traditional method and the needle (block arrowhead) can be punctured under real time scanning. This method is better than ultrasound guidance because flow of contrast can be seen during the injection and any communication from one compartment to another can be seen which suggests communicating tear. In this patient, contrast flow from the radiocarpal compartment to the distal radioulnar compartment through a defect in TFCC (long arrow). Contrast can also be seen flowing to the prestyloid recess (block arrow). No communication with the mid-carpal compartment; (B) ultrasound guidance of injection of diluted gadolinium into the radiocarpal joint. The needle can be identified by its echogenic linear appearance (block arrowheads). The tip can be seen contacting the distal radius; (C) after contrast injection into the both compartments, fluid distension of the radiocarpal and mid-carpal joints can be identified (asterisks). TFCC, triangular fibrocartilage complex.

there is a full thickness tear of the articular disc, the DRUJ will also distend and the proximal surface of the triangular fibrocartilage will be delineated by contrast. However, if there is not full-thickness communicating tear, then injection of contrast into the DRUJ is necessary. If only the radiocarpal joint is injected, one may overlook a partial thickness tear along the proximal surface of triangular fibrocartilage or a tear of the proximal lamina attaching to the ulnar fovea.

In ulnotriquetral and ulnolunate ligament tears, there is no inter-compartment communication and thus there is only capsular leakage of contrast material evident on arthrogram or MR arthrogram after contrast is injected into either the DRUJ or radiocarpal joint (24).

Indirect arthrography is possible since intravenous contrast will diffuse into the joint space after about 20 minutes. The more synovitis is present, the more likelihood of contrast accumulation within the joint fluid. Schweitzer *et al.* and Herold *et al.* showed this method to have a higher accuracy at depicting tears of the TFCC (21,22). However, no communication from one compartment to another can be demonstrated compared to real time screening of contrast injection under fluoroscopy.

MR imaging of the TFCC can also be performed with or without traction. The wrist traction device was set up with the finger traps applied to the index and ring fingers and connected to a preselected weight (7 kg for men and 5 kg for women) by a nonelastic cord. The cord is routed over the edge of the MRI gantry table. Traction is better following direct MR arthrography since this removes the vacuum effect pulling opposing bone surfaces together. Traction is still possible, nevertheless, without prior direct arthrography though the degree of distraction achieved is less. Traction helps further improve the depiction of TFCC, and intrinsic ligament tears as well as articular cartilage surface during MR imaging of the wrist. The current likely hierarchy of techniques for wrist imaging with respect to depiction of tears and articular cartilage surface is suggested (*Figure 4*).

High resolution standard (i.e., non-arthrographic) MR imaging of the wrist without traction is highly accurate in the depiction of most TFCC pathology, particularly with regard to determining whether surgery is necessary or not, and this is by far the most widely used approach for high quality wrist imaging in most clinical settings. The non-standard approaches (direct/indirect arthrography, traction) have been shown to add significant benefit in overall accuracy though their use should be reserved for pre-determined selected clinical cases.

## Normal appearances of TFCC

The central component of TFCC is a disc which is composed of fibrocartilage and shows homogeneous low signal intensity on spin-echo images (25) (*Figures 5,6*). Slightly increased in signal intensity on short TE sequences is related to mucoid degeneration, seen most commonly in elderly patients.

The triangular fibrocartilage disc is biconcave bowtie in appearance on coronal views, discoid on sagittal and triangular on axial images. It is thicker on the dorsal and volar sides.

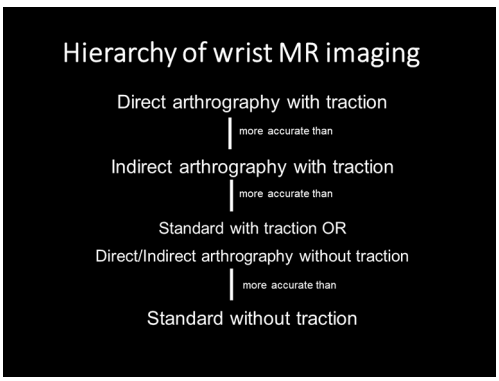


**Figure 4** The current likely hierarchy of techniques for wrist imaging with respect to depiction of tears and articular cartilage surface is suggested.

The thickness of the triangular fibrocartilage disc depends on the degree of ulnar variance (6). In the ulnar negative wrist, triangular fibrocartilage disc appears thick and short and lies horizontal. In the ulnar positive wrist, it appears thin and elongated and lies in a more vertical orientation. A thin triangular fibrocartilage disc is more vulnerable to tear.

The proximal and distal laminae appear striated in appearance, less homogeneous and low in signal on all sequences (*Figures 5,6*). The ligamentum subcruentum appears as a higher signal intensity on T1 and T2-weighted images in between the laminae (4). On the radial side, the triangular fibrocartilage is attached the cartilage rim of the distal radius which is a high signal on PD or T2W images.

Ulnomeniscal homologue is fat signal on MRI and lies just ulnar to the prestyloid recess (26). It is best seen on coronal imaging (*Figure 5B*).

The dorsal and ulnar radioulnar ligaments are most easily discerned on sagittal images (*Figure 6*). These are striated in appearance and represent the thickest part of the margin of the triangular fibrocartilage. They are homogeneous, of slightly higher signal intensity and are not easily separated from the triangular fibrocartilage (4).

The ulnotriquetral and ulnolunate ligament show homogeneous low signal intensity. They can be identified

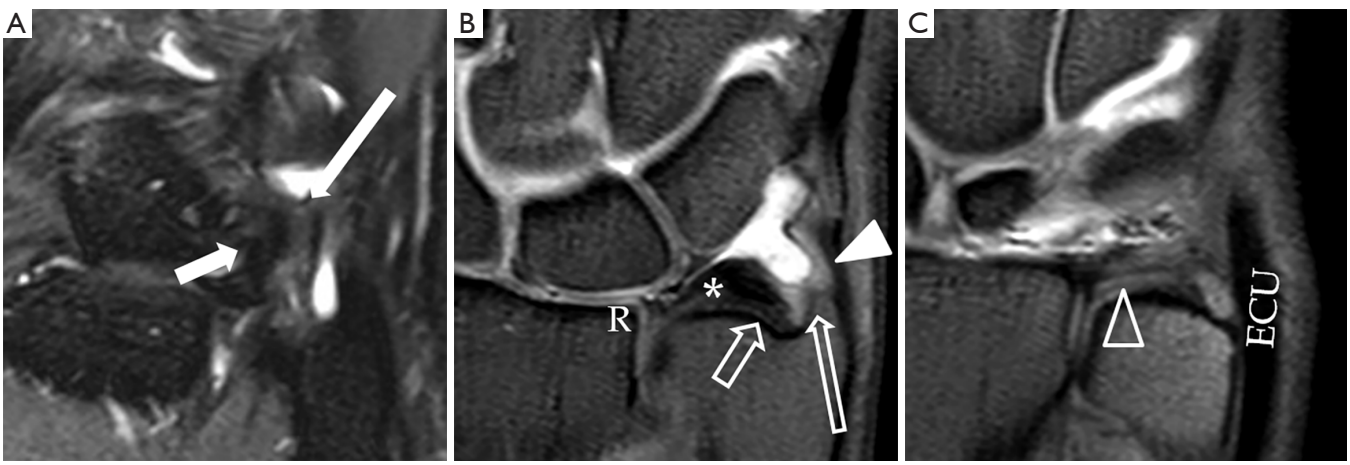


**Figure 5** Proton density fat-suppressed MR arthrography images showing the important components of the TFCC on coronal images from volar to dorsal. (A) Ulnotriquetral (long solid arrow) and ulnolunate ligaments (short solid arrow); (B) triangular fibrocartilage articular disc (TFC) (asterisk) with radial attachment (R), foveal attachment (short block arrow), ulnar styloid process attachment (long block arrow), meniscal homologue attachment (arrowhead); (C) most dorsal aspect of TFCC with dRUL (block arrowhead) and ECU tendon sheath attachment (ECU). Small low signal foci in the ulnocarpal joint which is due to small gas locules introduced during injection of contrast. TFCC, triangular fibrocartilage complex; dRUL, dorsal radioulnar ligaments; ECU, extensor carpi ulnaris.

 

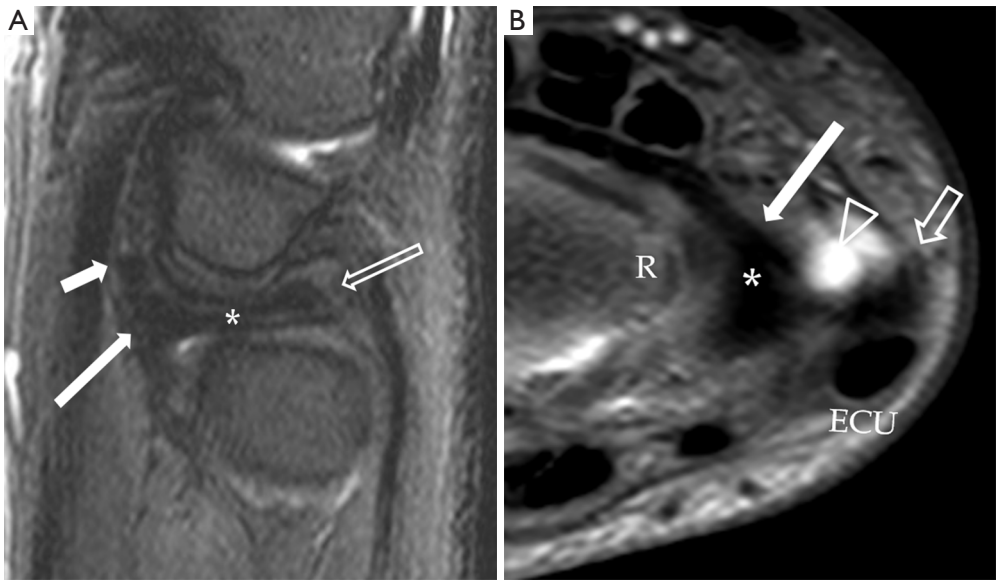


**Figure 6** Normal appearance of the TFCC on sagittal T2W fat-suppressed (A) and axial proton-density fat suppressed (B) images. (A) The TFC (asterisk) is concave in appearance on a sagittal view. On the volar side, the TFC is attaching to the volar radioulnar ligament (vRUL) (long solid arrow) and more distally through the ulnotriquetral ligament (short solid arrows). On the dorsal side, the TFC is attaching to the dorsal radioulnar ligament (block block arrow). These structures are not seen as distinct structures on MRI when they are normal; (B) the TFC (asterisk) is barely seen on axial image. On the volar side, the TFC is attaching to a low signal linear structure representing the volar radioulnar ligament (vRUL). On the radial side, it attaches to the distal radial cartilaginous rim (R). On the ulnar side, the attachments are very difficult to be appreciated at this level. However, the location of the distal ulnar styloid process (short block arrow) and the ECU can be appreciated on this image. Fluid within the pre-styloid recess is seen (arrowhead). TFCC, triangular fibrocartilage complex; ECU, extensor carpi ulnaris.

on coronal and sagittal images by tracing them from the triangular fibrocartilage to the lunate and triquetral bones on consecutive slices (24) (*Figures 5,6*).

## Types of TFCC tears

According to Palmer's classification, the TFCC tear is divided into traumatic (type 1) or degenerative (type 2) tear. Degenerative tear is not discussed in this manuscript which primarily focuses on traumatic tears. Traumatic tears are divided into A to D (*Figure 7*).

- 1A tear is at the central or paracentral region of the triangular fibrocartilage. It is usually situated at the paracentral region, ~2–4 mm from the radial attachment;
- 1B is avulsion tear at the ulnar attachment with or without an ulnar styloid fracture. The tear is either at the ulnar styloid process attachment or the foveal attachment;
- 1C is avulsion tear at the distal attachment at the lunate or triquetrum i.e., the ulnolunate and ulnotriquetral ligament with or without avulsion fracture;
- 1D is avulsion tear at the radial attachment with or without distal radial fracture.

The type of treatment is mainly dependent on the blood supply. For 1A tear, since this part of the articular disc is avascular, no repair can be done and only debridement is performed. For 1B and 1C tears, the area of tear is vascularized and surgical repair can obtain good result. The current trend is to repair the TFCC under arthroscopy (27,28). For 1D tear, there are various ways to repair, depending on any associated ligament tear and DRUJ instability. In some cases, ulnar shortening osteotomy or arthroscopic wafer ulnar resection will be performed for relieving the axial load and stress on the TFCC.

## Limitations of palmar classification

This classification has its limitations. The TFCC tear at the volar/dorsal radioulnar ligaments are not categorized under Palmer's classification (29). Type 1B tear have not been further subclassified as tears of the foveal attachment,

 

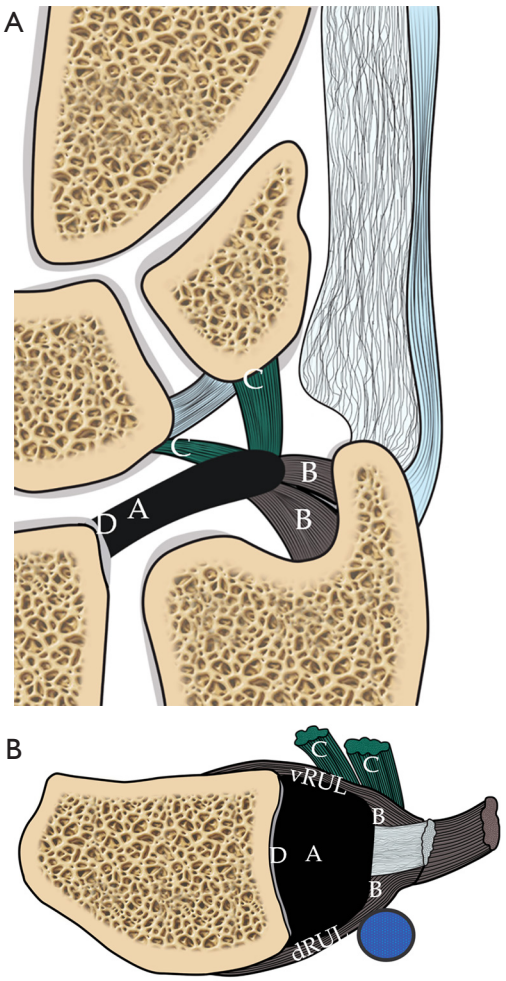


**Figure 7** Schematic diagram showing the Palmar classification of TFCC tears. (A) Coronal view shows the different types of tear correspond to the location of the tear. Type 1A is central TFC perforation. 1B, peripheral ulnar side TFCC tear (± ulna styloid fracture). 1C, distal TFCC disruption (disruption of distal UC ligaments) and 1D, radial TFCC disruption (± sigmoid notch fracture); (B) axial view shows the different tear locations. A tear on the volar and dorsal sides of the TFC involving the volar (vRUL) or dorsal radioulnar ligament (dRUL) is not included in the Palmar classification. TFCC, triangular fibrocartilage complex.

ulnomeniscal homologue, ulnar collateral ligament or ECU subsheath. Thirdly, there is no further differentiation into the full thickness or partial thickness tear or into different tear configuration, e.g., flap, horizontal tear (5,29). Finally, combined tear is not included which is not uncommon. Abe *et al.* found that there were 32 combined tears in 173 wrists (18.5%) (29).

## MRI features of TFCC tear

Tear is defined as fluid signal intensity extending through the disc or ligament on fluid sensitive sequences, including proton density, T2-weighted or gradient echoes sequences (30). The tear can be a radial tear or named as slit-like radial or vertical appearance i.e., parallel to the rim of the distal radius or it can be horizontal in appearance. Combined tear or complex tear is not uncommon which include two components.

Palmer 1A tear is common. A slit tear at the central and paracentral region of the triangular fibrocartilage (*Figure 8*). The tear can be partial-thickness tear or full-thickness tear. Partial thickness tear only involves one articular surface, usually the proximal surface. MR arthrography of the DRUJ is good to depict this often subtle tear.

Palmer 1B tear is an avulsion of either the proximal or distal lamina (*Figure 9*). This peripheral tear is the most commonly missed. Indirect clues include altered morphology, excessive fluid accumulation and focal synovitis around this region (31). MR arthrography of the DRUJ will also help to depict tears at the foveal attachment.

Ulnar detachment can be associated with avulsion fracture at the base of the styloid process (32,33) (*Figure 10*). Non-united styloid fracture in chronic TFCC tear with DRUJ instability is not uncommon.

Other secondary signs include the extension of fluid along the medial border of distal ulna, avulsive cystic changes or bone marrow oedema of the ulnar styloid process and fovea, and fascial oedema and fluid (3).

Palmer 1C tear is avulsion tear at the distal attachments of the lunate or triquetral bone (*Figure 11*). Tears of the UTL and ULL are usually intrasubstance tears with oedema and thickening rather than fibre discontinuity. The normal UTL and ULL are sometimes lax and slightly increased signal (2) on short TE sequence. If abnormal signal is seen within the ligaments on fluid-sensitive sequences, then a tear is likely (34).

Palmer 1D tear is avulsion tear at the radial attachment ± distal radial sigmoid fracture (*Figure 12*). Palmer 1D tear is either avulsion tear of the TFCC or avulsion fracture at the radial rim. When there is a tear at the radial side, it is important to look for any remnant attaching to the radial rim. If there is a small remnant present, it is termed a type 1A rather than 1D tear (4).

As mentioned in the previous paragraphs, the TFCC tear can be found at the dorsal radioulnar ligament (*Figure 13*), at the volar side (*Figure 14*) or at the ulnomeniscal homologue (*Figure 15*) which are not under the classification

 

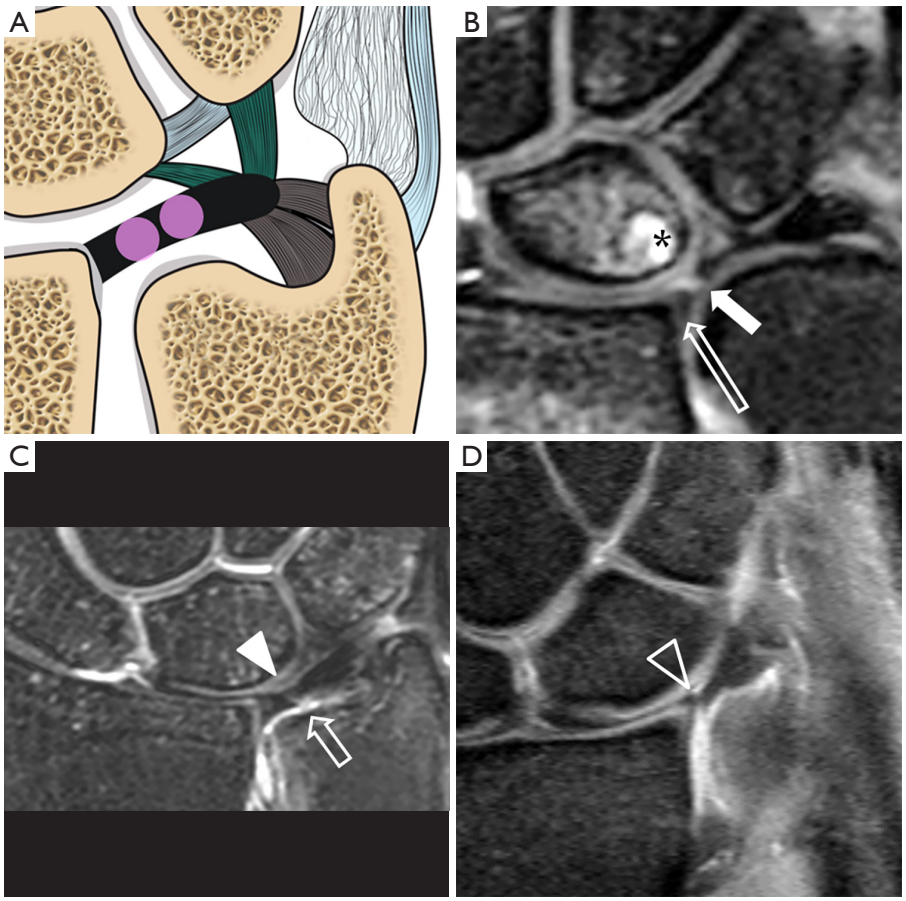


**Figure 8** Type 1A tear. (A) Schematic drawing showing the tear (pink circle) at the central or paracentral part of the TFCC. Proton density fat suppression Coronal MRI images showing (B) full thickness tear with a small gap filled with fluid (short solid arrow). There is a small remnant of TFC at the radial attachment (long block arrow). A small subchondral cyst is at the proximal ulnar side of the lunate bone (asterisk); (C) partial thickness tear at the undersurface of the TFC (short block arrow). The distal surface of TFC is intact with the contour preserved (solid arrowhead); (D) contour irregularity (block arrowhead) of the TFC is also a sign of TFC tear as in this case which was confirmed to be a communicating full thickness tear during arthroscopy. TFCC, triangular fibrocartilage complex.

of Palmer's classification. Some of tears are atypical in tear configuration or in combination (*Figure 16*).

Since some of the TFCC tears will result in DRUJ instability (1B to 1D) (29,35), the congruity of the ulnar head within the sigmoid notch will be disrupted, causing dorsal or volar subluxation. Dorsal instability is more common. A lateral radiograph or a CT scan can be used to confirm dorsal subluxation in neutral position (36). Mild dorsal subluxation may only manifest on pronation and volar subluxation on supination. For detailed evaluation, a CT scan performed in the neutral, pronation and supination positions is helpful. Usually both wrists are examined simultaneously as some individuals simply have undue physiological laxity and in this instance a comparable degree of laxity will be apparent on both sides. Chronic instability of DRUJ will predispose DRUJ degenerative change (*Figure 17*).

An ulnar positive variant is more frequently seen in patients with TFCC tear because this leads to developmental thinning of the articular disc with increase in force borne by the distal portion of the ulna (37). Ulnocarpal impaction may also be seen in these patients as evident by cartilage thinning or focal cartilage loss at the ulnar proximal aspect of the lunate (*Figure 18*), associated lunate bone oedema and attrition tears of the luno-triquetral ligament.

It is difficult to differentiate between degenerative and traumatic tears. The features favouring degenerative tears include diffuse thinning of the triangular fibrocartilage, ulnar positive variant, site of tear closer to the radial

 

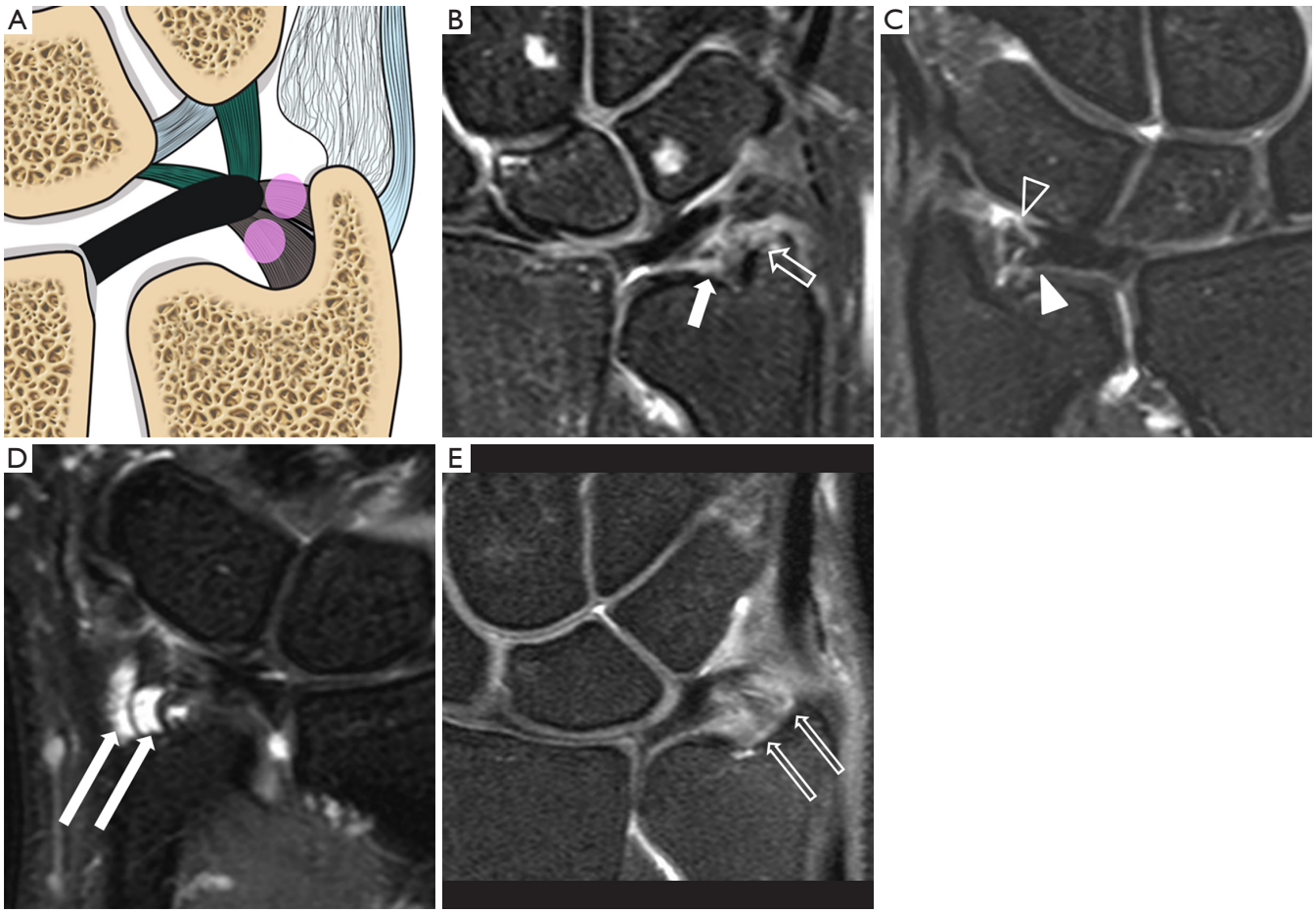


**Figure 9** Type 1B tear. (A) Schematic drawing showing the tear (pink circles) at the proximal and distal laminae of TFCC which attach to the ulnar fovea and distal ulnar styloid process respectively. Proton-density fat-suppressed coronal MRI images showing (B) full-thickness tear as evident by complete loss of fibres of proximal (short solid arrow) which are expected to attach to the fovea and the distal ulnar styloid process; (C) another patient with a full thickness tear at the proximal (solid arrowhead) and distal laminae (block arrowhead) as evidenced by fibre discontinuity. During arthroscopy, a hook sign and trampoline effect are suggestive of unstable tear of the TFCC. Trampoline sign is positive when TFCC is soft and lax while hook test is positive when the TFCC can be pulled upward and radially towards the center during the arthroscopy using the probe. They are indicative of peripheral tear and foveal tear respectively; (D) cystic changes within the proximal and distal laminae of the TFCC attachments (long solid arrows) due to intrasubstance partial tear; (E) oedematous and thickened fibres of the proximal and distal lamina (long block arrows) due to high grade partial tear. Overall lamina continuity seems to be maintained. TFCC, triangular fibrocartilage complex.

attachment. Both types of tear frequently co-exist.

## Accuracy of MRI in TFCC tear detection

### *Plain MRI scan*

Standard MRI can achieve high performance in detection of the TFCC tear. In a recent study, Zlatkin *et al.* found that the sensitivity, specificity and accuracy was 92%, 89% and 91% respectively (4). Johnstone and coworkers *et al.* also found that the sensitivity and specificity was 90% and 70% respectively (38). Haims *et al.* found that synovitis can be used as a marker for ulnar-sided tear (31) though the sensitivity and specificity are not high, which was 42% and 63% respectively. Oneson *et al.* found that sensitivity and specificity of radial slit-like tear was 100% and 86% though diagnosis of ulnar-sided tear was not so high (39).

Potter *et al.* have tried to use 3D-gradient echoes thin

 


**Figure 10** Type 1B tear. (A) Injury one week prior. Proton-density coronal MRI image showing moderately displaced fracture base of ulnar styloid process (short solid arrow). The distal lamina is partially torn (short block arrow) with a complete tear of the proximal lamina (solid arrowhead); (B) frontal radiograph shows fracture of ulnar styloid process (block arrowhead). The TFCC cannot be evaluated radiographically; (C) proton density fat-suppressed coronal MRI image shows avulsion fracture of distal ulnar styloid process (long solid arrow). The distal laminar fibres are intact (long block arrow) though mild increased abnormal signal suggests mild sprain. A complete tear of the proximal lamina fibres (curved solid arrow) is also present. TFCC, triangular fibrocartilage complex.

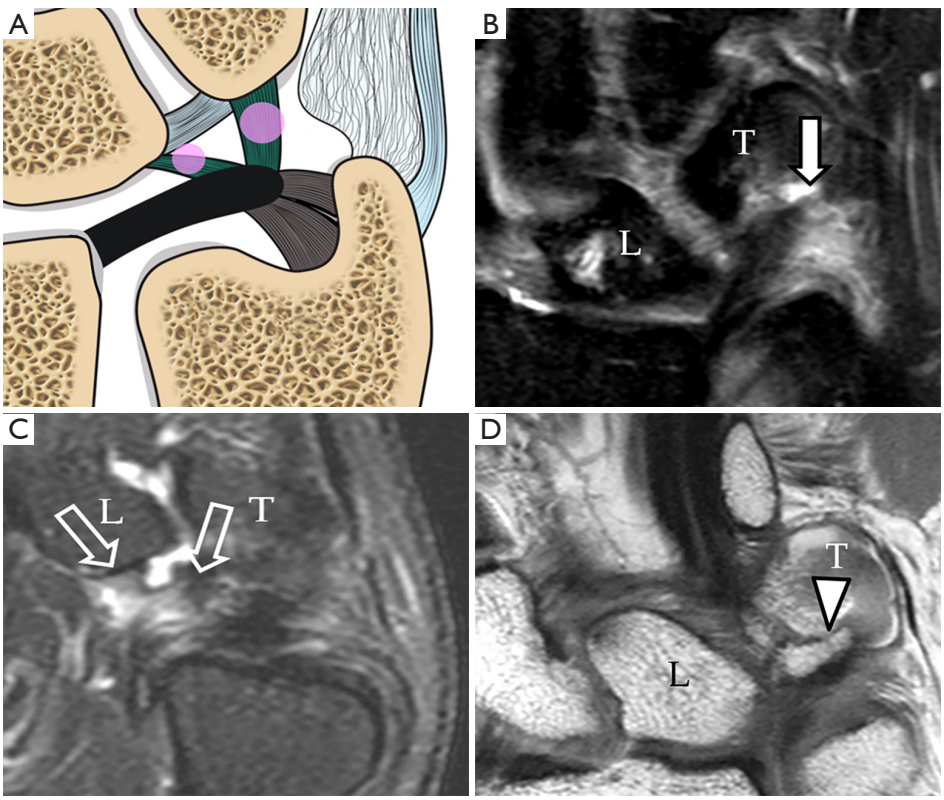


**Figure 11** Type 1C tear. (A) Schematic drawing showing tear of the ulnolunate and ulnotriquetral ligaments (pink circles); (B) proton density fat suppressed coronal MRI image shows severe oedematous change with thickening at the ulnotriquetral ligament (short solid arrow) consistent with a intrasubstance partial tear of this ligament; (C) proton-density fat suppression coronal MRI image of another patient showed severe oedematous change with thickening at the ulnolunate ligament (short block arrows) attaching to proximal lunate (L) consistent with an intrasubstance partial tear; (D) proton-density coronal MRI image of another patient shows avulsion fracture of proximal triquetrum (T) at the attachment of the ulnotriquetral ligament (solid arrowhead).

 

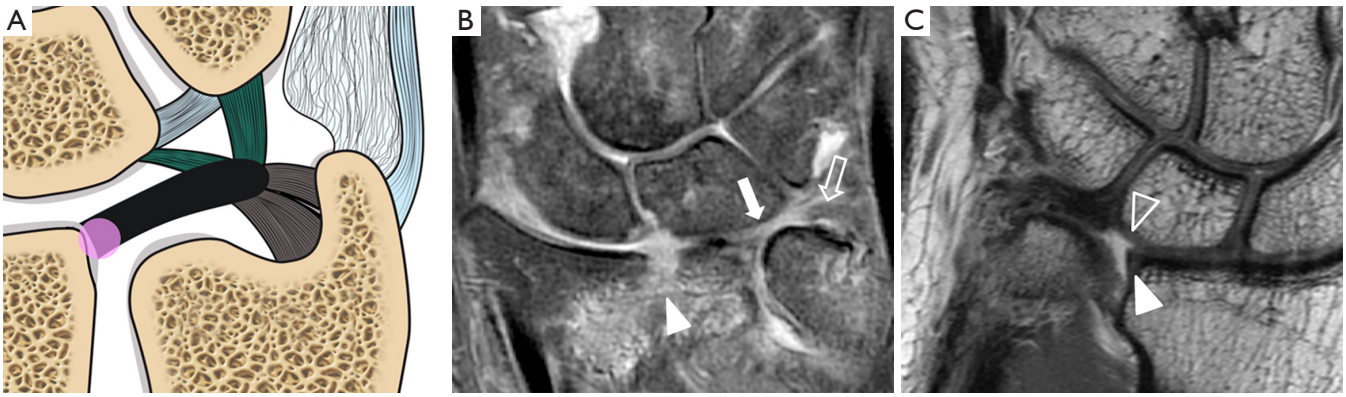


**Figure 12** Type 1D tear. (A) Schematic drawing showing tear at the radial attachment (pink circle); (B) proton density fat-suppressed coronal MRI image shows an avulsion tear present at the radial attachment (short solid arrow). Peripheral retraction of the TFCC is noted (short block arrow). This patient had history of fracture distal radius with intraarticular extension (solid arrowhead); (C) proton density coronal MRI of another patient showed avulsion tear at the radial attachment (solid arrowhead) associated with peripheral retraction of the TFC leaving a gap filled up with fluid (block arrowhead). There is no remnant of the TFC at the radial attachment to suggest type 1A tear. TFCC, triangular fibrocartilage complex.

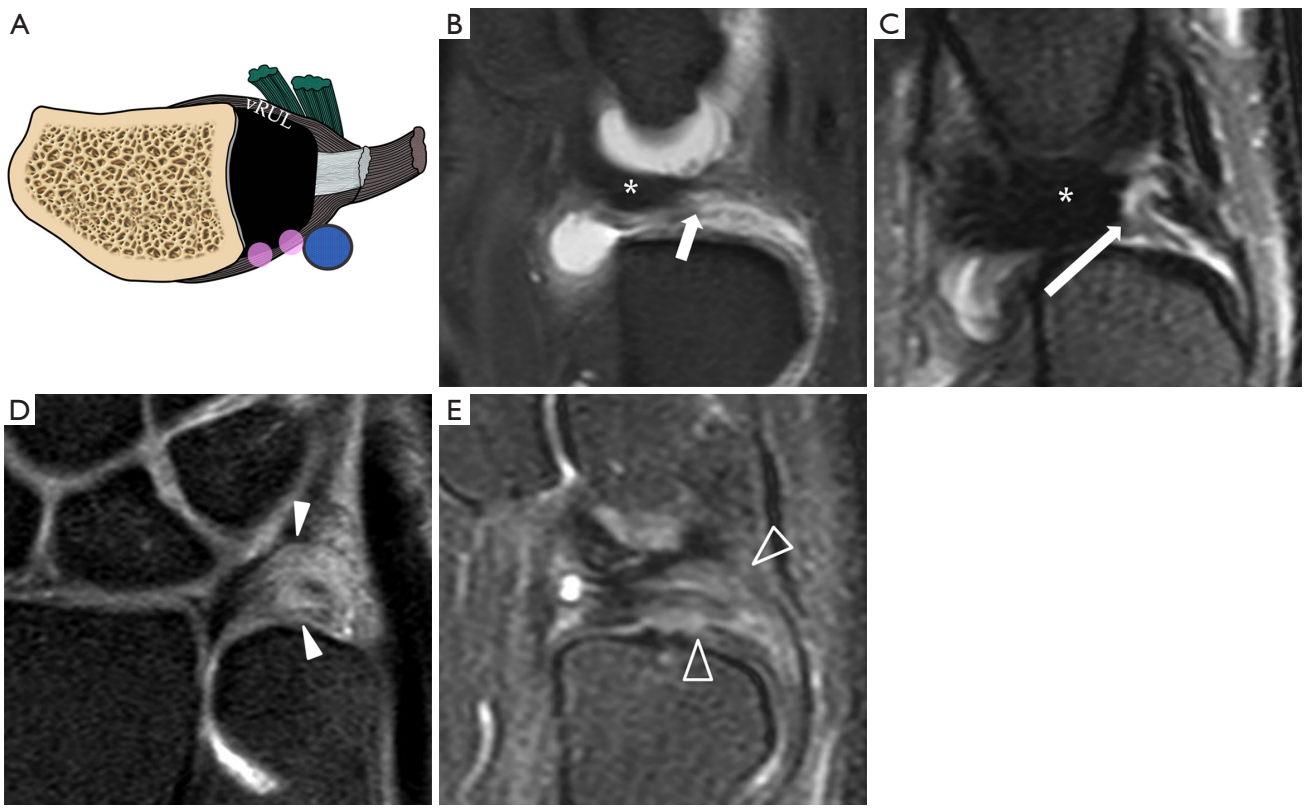


**Figure 13** Dorsal sided TFCC tear. (A) Schematic drawing showing tear at the dorsal radioulnar ligament (pink circles); (B) sagittal T1W fat-suppressed MR arthrogram image shows a partial tear on the dorsal side of the TFC (solid arrow); (C) sagittal proton density fat suppressed coronal MRI image shows almost complete detachment of the TFCC at the dorsal radioulnar ligament (solid arrow); (D) proton density fat-suppressed coronal MRI image showing a severely oedematous and thickened dorsal radioulnar ligament (solid arrowheads) due to severe partial tear; (E) T2-weighted fat suppressed sagittal MRI image of another patient showing moderate thickening and oedema of the dorsal radioulnar ligament due to a severe partial tear (block arrowheads). TFCC, triangular fibrocartilage complex.

 

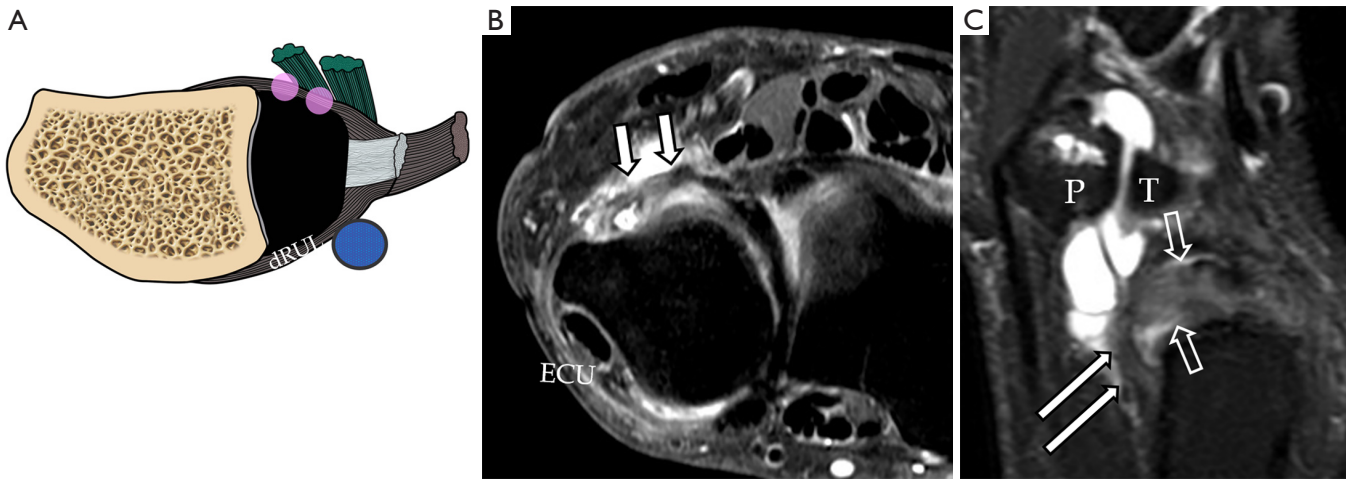


**Figure 14** Volar sided TFCC tear. (A) Schematic drawing depicting a tear of the volar radioulnar ligament (pink circles); (B) T1-weighted fat-suppressed axial MR arthrogram shows thickened, oedematous severely torn volar radioulnar ligament (short solid arrows); (C) corresponding sagittal T1-weighted fat suppressed MR arthrogram shows this thickened and oedematous volar radioulnar ligament (long solid arrows) is still attached to the TFC which itself is also thickened and oedematous consistent with severe partial tear (block arrows). P, pisiform; T, triquetral. ECU, extensor carpi ulnaris; TFCC, triangular fibrocartilage complex.

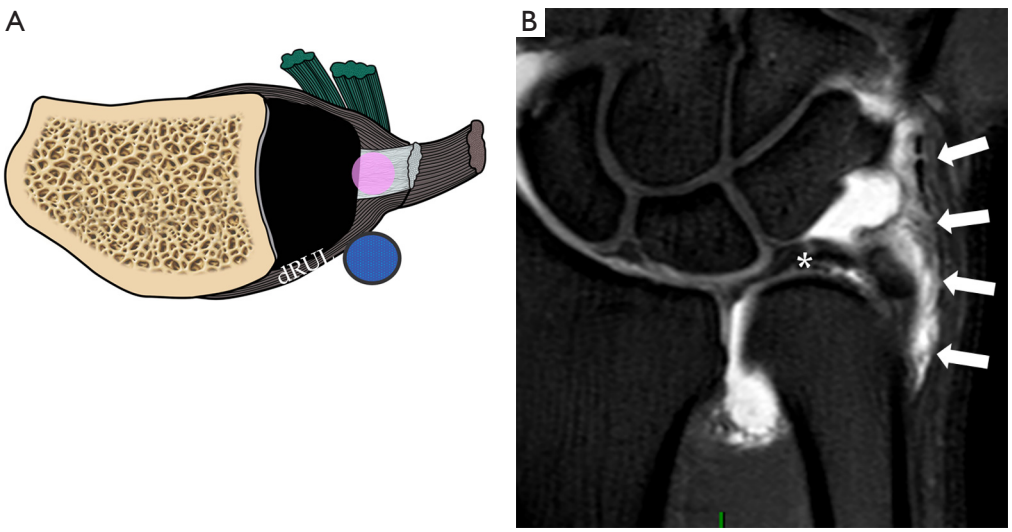


**Figure 15** Ulnomeniscal homologue tear. (A) Schematic drawing depicting a tear at the ulnomeniscal homologue (pink circle); (B) coronal T1-weighted fat-suppressed MR arthrogram showing partial tear at the ulnomeniscal homologue (solid arrows) extending from the distal ulnar attachment proximally to the triquetral attachment distally. The detachment of the ulnomeniscal homologue to the periphery of TFC (asterisk) can be appreciated. TFCC, triangular fibrocartilage complex.

 

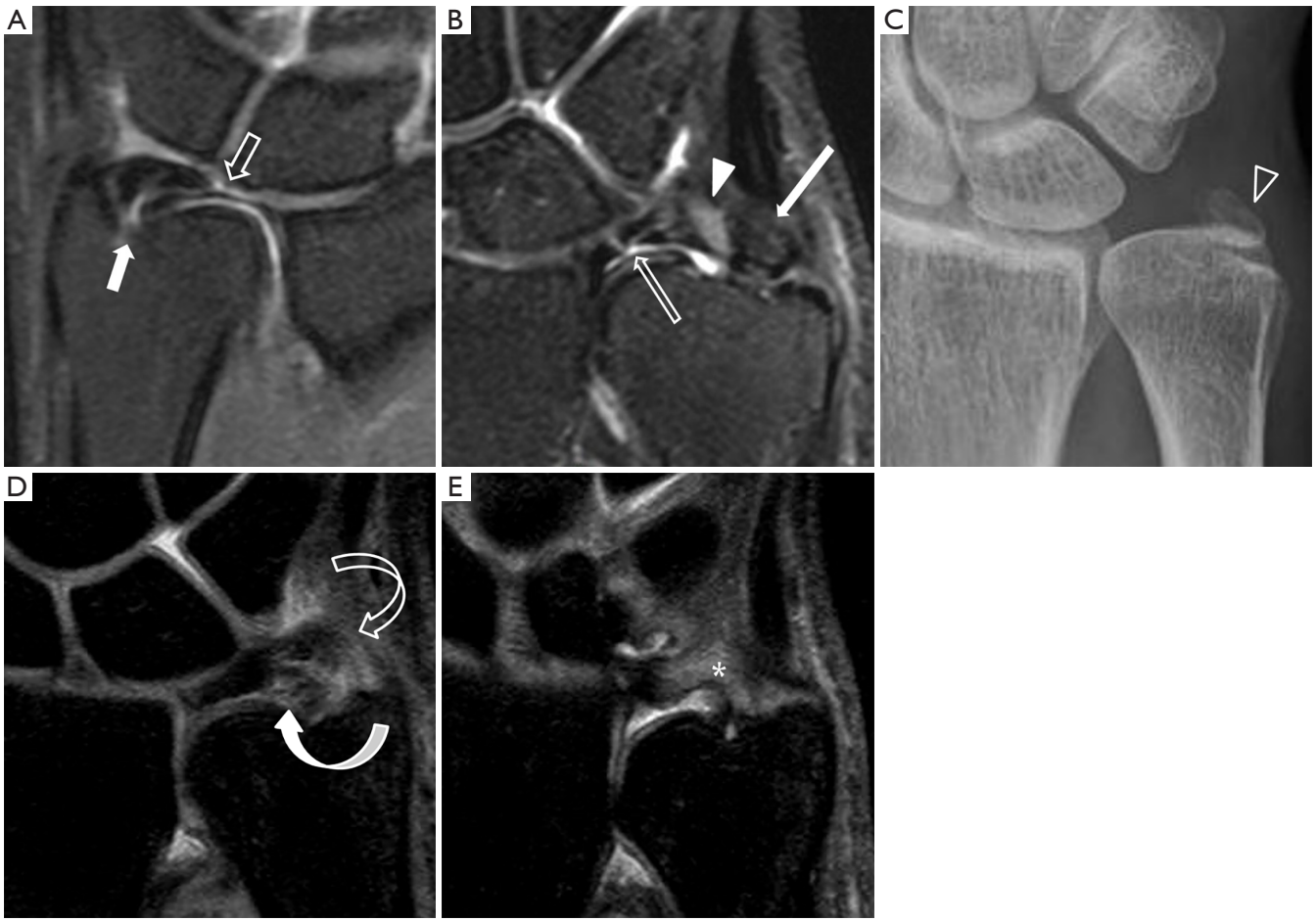


**Figure 16** Atypical TFCC tear. (A) Coronal proton density fat-suppressed MR image shows atypical tear of the TFC centrally located and extending from the distal surface (block arrow) to the foveal attachment (solid arrow). This is due to a combination of Palmar classification type 1A and type 1B tears; (B) coronal proton-density fat suppressed MR image shows chronic avulsion fracture at the base of distal ulnar styloid process (solid long arrow). Associated with abnormal high signal in the attachment of TFCC (solid arrowhead). Features are compatible with Type 1B tear. There is also a small linear tear at the paracentral portion of the TFC (block long arrow) compatible with type 1A tear; (C) frontal radiograph of the same patient shows the non-united fracture at the base (block arrowhead) of the ulnar styloid process (type 2). Type 2 fracture is usually associated with TFCC disruption and DRUJ instability. About 65% of patients have non-union of ulnar styloid fractures; (D) coronal proton density fat-suppressed MR image in a patient with DRUJ instability clinically showing a severe partial tear of the proximal (curved solid arrow) and distal laminae (block curved arrow) at the styloid and foveal attachments respectively; (E) in the same patient more dorsally, there is a severe sprain of the dorsal radioulnar ligament with thickening and oedema (asterisk). TFCC, triangular fibrocartilage complex; DRUJ, distal radioulnar joint.

 

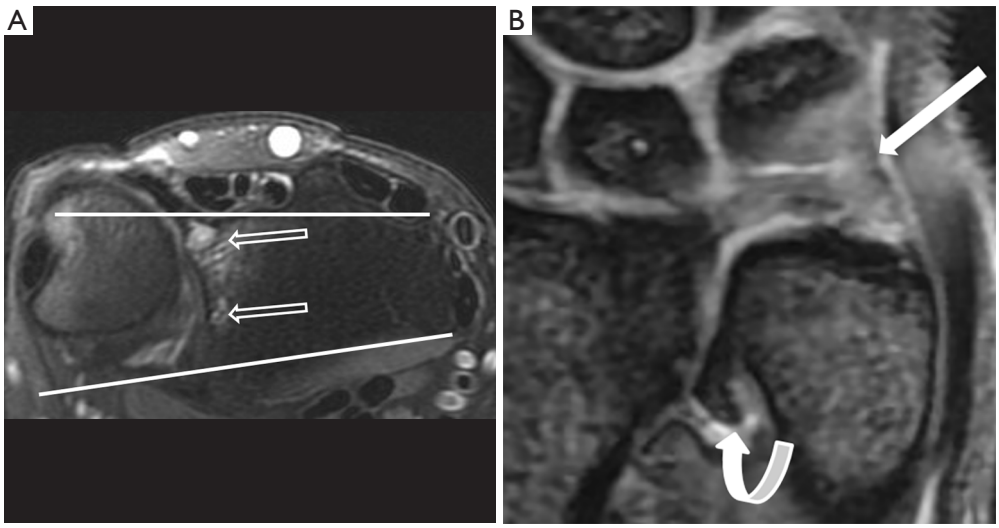


**Figure 17** Dorsal subluxation of the DRUJ. (A) Axial proton density fat-suppressed MR image. There is dorsal subluxation of the distal ulna at the sigmoid notch associated with moderate subchondral cystic changes (block long arrows) of the radius; (B) coronal proton density fat-suppressed MR image of another patient showed an ulnar-sided tear of the TFCC (solid long arrow). There is severe degeneration of the DRUJ with osteophytes (solid curved arrow) and joint effusion due to chronic DRUJ instability. TFCC, triangular fibrocartilage complex; DRUJ, distal radioulnar joint.

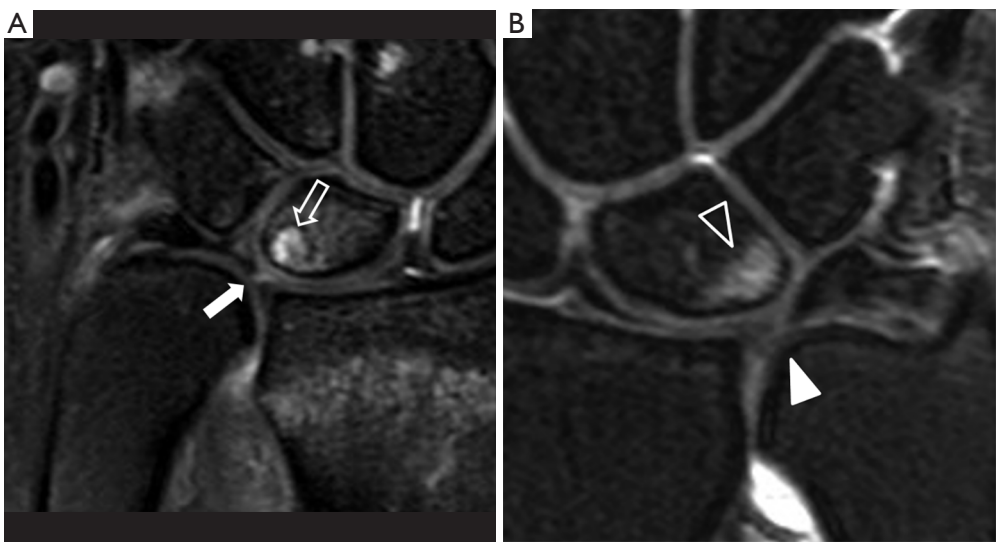


**Figure 18** Ulnocarpal impaction. (A) Coronal proton density fat-suppressed MR image shows type 1a paracentral region tear (solid arrow) associated with subchondral cystic changes on the ulnar proximal aspect of the lunate (block arrow) consistent with ulnocarpal impaction. Mild ulnar positive variance is present; (B) coronal proton density fat-suppressed MR image of another patient also shows type 1a tear at the paracentral region of the TFCC (solid arrowhead) associated with subchondral cystic changes on the ulnar proximal aspect of the lunate (block arrowhead) with mild overlying cartilage irregularity. Features consistent with ulnocarpal impaction. TFCC, triangular fibrocartilage complex.

 

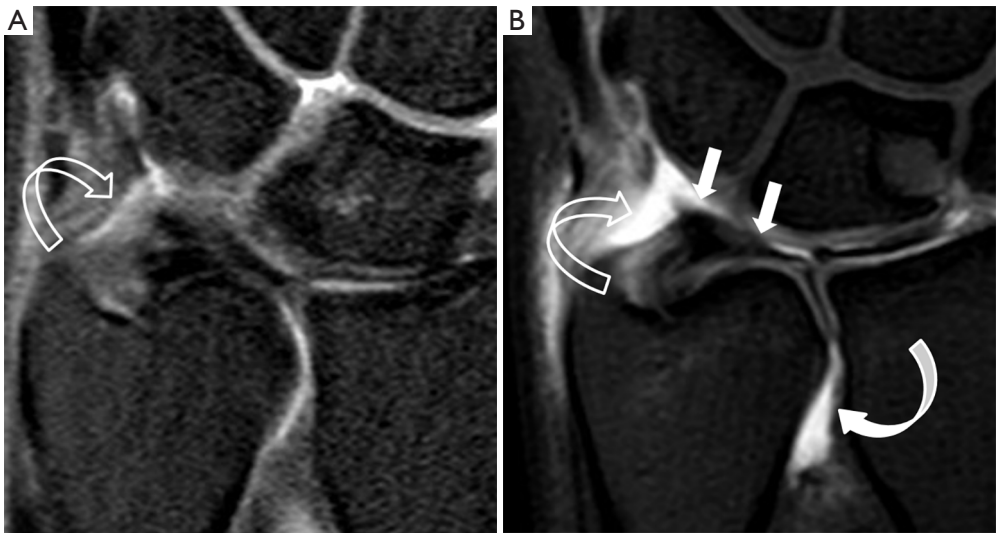


**Figure 19** Comparison of TFCC visualization by non-arthrogram MRI (A) and MR arthrogram (B). Before injection of contrast, the prestyloid recess (block curved arrow) is not distended and the radiocarpal joint surface of TFCC cannot be well delineated. After contrast injection into the joint, the joints are well distended including the prestyoid recess (block curved arrow) and DRUJ (solid curved arrow). The surface of the TFCC can now be well delineated (solid arrows). TFCC, triangular fibrocartilage complex; DRUJ, distal radioulnar joint.

slices to improve the diagnosis of TFCC tear showing how MRI could achieve sensitivity and specificity up to 100% and 90% respectively (19).

### *MR arthrography*

MRA was considered better than standard MR to depict central and peripheral tears with sensitivity and specificity more than 90% (40-43) (*Figure 19*).

Rarely, false negative diagnoses may occur for communicating tear when scar and fibrosis block the flow of contrast through the defect (44).

Herold *et al.* studied 45 patients and found that MR arthrogram using an indirect arthrogram method is better to detect TFCC defect with a sensitivity, specificity and accuracy of indirect arthrography were 100%, 77% and 93% respectively (22). Schweitzer *et al.* also found that MR arthrogram could achieve 100% accuracy though the sample size is small (21). However, some authors found that there is no significant difference when compared to non-enhanced MRI scan (45).

### *Multi-detector computed tomography (MDCT) arthrography*

MDCT arthrography was advocated as an alternative to MR arthrography for its better resolution but its potential benefit is still controversial (23,46,47).

### *MR wrist with traction*

Recently, MR wrist traction was proven to have significantly improved the visibility and detection of TFCC tears. The accuracy of TFCC tear has increased from 83% to 98% (48) (*Figure 20*). MR with traction is well tolerated and does not increase the examination time too much as almost all the preparation work is completed before entering the scanning room (48).

## Pitfalls of MRI in TFCC tear detection

Mucoid degeneration will render the TFCC high signal intensity on short TE sequence, i.e., T1-weighted and proton-density sequences simulating tears (49). This alteration in signal intensity reflects alteration in the water binding property of the TFCC disk (50).

The most difficult area for detection of TFCC tears is the peripheral tear at the ulnar side, at the ulnar styloid and foveal attachements, especially for low field MRI studies (39). Haims *et al.* found that the sensitivity, specificity and accuracy of detection of peripheral ulnar tear were only 17%, 79% and 64% only (31).

 

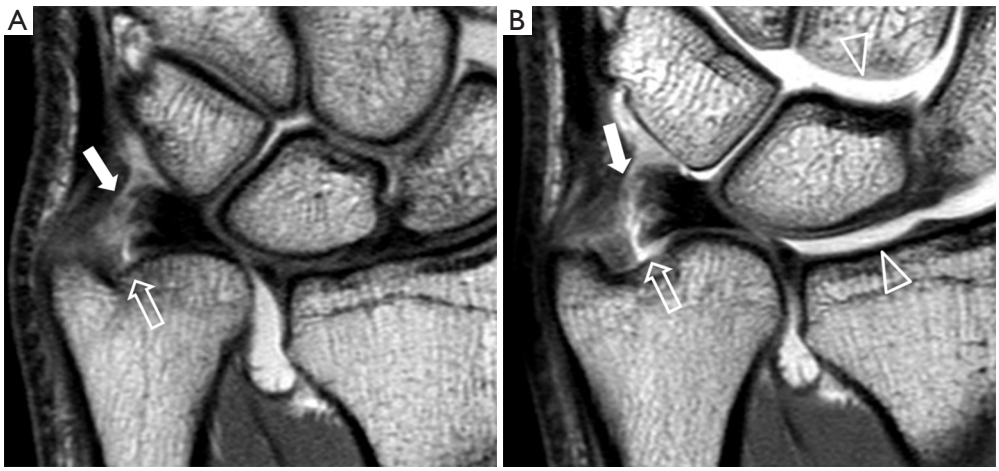


**Figure 20** Comparison of TFCC visualization using non-traction MRI (A) and traction MRI (B). Before traction, there is a tear depicted at the foveal attachment (block arrow) of the TFCC but the styloid attachment appears intact (solid arrow). After traction, discontinuity at the styloid attachment can be fully appreciated (solid arrow). The radiocarpal and the mid-carpal joints are widened following traction (arrowheads). TFCC, triangular fibrocartilage complex.

The ligamentum subcruentum is loose areolar tissue situated between the proximal and distal laminae. It appears intermediate or slightly high T2W or proton density signal and this can mimic a tear in this region (51,52).

The attachment of the TFCC at the radial articular cartilage, which appears hyperintense on proton and T2W sequences, can also mimic a tear (52) but is easy to recognize once you are aware of this pitfall. Peripheral and undersurface tears of the triangular fibrocartilage can be obscured by synovitis (4). MR arthrogram is useful to differentiate a tear or synovitis if it cannot be differentiated by plain MRI.

## Conclusions

MRI imaging is extremely helpful in revealing the normal anatomy and injury to the TFCC. Nowadays, with high or medium-field strength MR systems, high accuracy can be achieved in detecting and characterizing the specific type of injury present. Good quality MR imaging acquisition is a pre-requisite as it allows careful interpretation of the TFCC by a radiologist familiar with the normal MR anatomy of the TFCC as well as the likely injuries that can occur. In most instances, a standard high-resolution MR examination will suffice. Though in particular clinical settings, such as in professional athletes, MR arthrography and traction will help to maximize accuracy in those situations where doubt still exists after standard MR imaging.

## Acknowledgements

None.

## Footnote

*Conflicts of Interest*: The authors have no conflicts of interest to declare.

## References

1. Yu JS, Habib PA. Normal MR imaging anatomy of the wrist and hand. Radiol Clin North Am 2006;44:569-81.
2. Davis KW, Blankenbaker DG. Imaging the ligaments and tendons of the wrist. Semin Roentgenol 2010;45:194-217.
3. Chhabra A, Soldatos T, Thawait GK, Del Grande F, Thakkar RS, Means KR Jr, Carrino JA. Current perspectives on the advantages of 3-T MR imaging of the wrist. Radiographics 2012;32:879-96.
4. Zlatkin MB, Rosner J. MR imaging of ligaments and triangular fibrocartilage complex of the wrist. Radiol Clin North Am 2006;44:595-623
5. Watanabe A, Souza F, Vezeridis PS, Blazar P, Yoshioka H. Ulnar-sided wrist pain. II. Clinical imaging and treatment. Skeletal Radiol 2010;39:837-57.
6. Vezeridis PS, Yoshioka H, Han R, Blazar P. Ulnar-sided wrist pain. Part I: anatomy and physical examination. Skeletal Radiol 2010;39:733-45.

 

7. Nakamura T, Makita A. The proximal ligamentous component of the triangular fibrocartilage complex. J Hand Surg Br 2000;25:479-86.
8. Golimbu CN, Firooznia H, Melone CP Jr, Rafii M, Weinreb J, Leber C. Tears of the triangular fibrocartilage of the wrist: MR imaging. Radiology 1989;173:731-3.
9. Yoshioka H, Ueno T, Tanaka T, Shindo M, Itai Y. High-resolution MR imaging of triangular fibrocartilage complex (TFCC): comparison of microscopy coils and a conventional small surface coil. Skeletal Radiol 2003;32:575-81.
10. Palmer AK, Glisson RR, Werner FW. Relationship between ulnar variance and triangular fibrocartilage complex thickness. J Hand Surg Am 1984;9:681-2.
11. Smith DK. Volar carpal ligaments of the wrist: normal appearance on multiplanar reconstructions of three-dimensional Fourier transform MR imaging. AJR Am J Roentgenol 1993;161:353-7.
12. Taleisnik J. The ligaments of the wrist. J Hand Surg Am. 1976;1:110-8.
13. Prendergast N, Rauschning W. Normal anatomy of the hand and wrist. Magn Reson Imaging Clin N Am 1995;3:197-212.
14. Theumann NH, Pfirrmann CW, Antonio GE, Chung CB, Gilula LA, Trudell DJ, Resnick D. Extrinsic carpal ligaments: normal MR arthrographic appearance in cadavers. Radiology 2003;226:171-9.
15. Taleisnik J, Gelberman RH, Miller BW, Szabo RM. The extensor retinaculum of the wrist. J Hand Surg Am 1984;9:495-501.
16. Berquist TH. Anatomy. In: Berquist TH, editor. MRI of the hand and wrist. Philadelphia: Lippincoott Williams & Wilkins; 2003:1-32.
17. Thiru RG, Ferlic DC, Clayton ML, McClure DC. Arterial anatomy of the triangular fibrocartilage of the wrist and its surgical significance. J Hand Surg Am 1986;11:258-63.
18. Saupe N, Prüssmann KP, Luechinger R, Bösiger P, Marincek B, Weishaupt D. MR imaging of the wrist: comparison between 1.5- and 3-T MR imaging--preliminary experience. Radiology 2005;234:256-64.
19. Potter HG, Asnis-Ernberg L, Weiland AJ, Hotchkiss RN, Peterson MG, McCormack RR Jr. The utility of high-resolution magnetic resonance imaging in the evaluation of the triangular fibrocartilage complex of the wrist. J Bone Joint Surg Am 1997;79:1675-84.
20. Bae WC, Ruangchaijatuporn T, Chang EY, Biswas R, Du J, Statum S, Chung CB. MR morphology of triangular fibrocartilage complex: correlation with quantitative MR and biomechanical properties. Skeletal Radiol 2016;45:447-54.
21. Schweitzer ME, Natale P, Winalski CS, Culp R. Indirect wrist MR arthrography: the effects of passive motion versus active exercise. Skeletal Radiol 2000;29:10-4.
22. Herold T, Lenhart M, Held P, Babel M, Ruf S, Feuerbach S, Link J. Indirect MR Arthrography of the wrist in the diagnosis of TFCC-Lesions. Rofo 2001;173:1006-11.
23. Lee RK, Ng AW, Tong CS, Griffith JF, Tse WL, Wong C, Ho PC. Intrinsic ligament and triangular fibrocartilage complex tears of the wrist: comparison of MDCT arthrography, conventional 3-T MRI, and MR arthrography. Skeletal Radiol 2013;42:1277-85.
24. Resnick DL, Kang HS, Pretterklieber ML. Wrist and Hand. In: Internal derangements of Joints. 2nd edition. Saunders 2006:1218-418.
25. Sofka CM, Potter HG. Magnetic resonance imaging of the wrist. Semin Musculoskelet Radiol 2001;5:217-26.
26. Buck FM, Gheno R, Nico MA, Haghighi P, Trudell DJ, Resnick D. Ulnomeniscal homologue of the wrist: correlation of anatomic and MR imaging findings. Radiology 2009;253:771-9.
27. Tse WL, Lau SW, Wong WY, Cheng HS, Chow CS, Ho PC, Hung LK. Arthroscopic reconstruction of triangular fibrocartilage complex (TFCC) with tendon graft for chronic DRUJ instability. Injury 2013;44:386-90.
28. Estrella EP, Hung LK, Ho PC, Tse WL. Arthroscopic repair of triangular fibrocartilage complex tears. Arthroscopy 2007;23:729-37.
29. Abe Y, Tominaga Y, Yoshida K. Various patterns of traumatic triangular fibrocartilage complex tear. Hand Surg 2012;17:191-8.
30. Zlatkin MB, Chao PC, Osterman AL, Schnall MD, Dalinka MK, Kressel HY. Chronic wrist pain: evaluation with high-resolution MR imaging. Radiology 1989;173:723-9.
31. Haims AH, Schweitzer ME, Morrison WB, Deely D, Lange R, Osterman AL, Bednar JM, Taras JS, Culp RW. Limitations of MR imaging in the diagnosis of peripheral tears of the triangular fibrocartilage of the wrist. AJR Am J Roentgenol 2002;178:419-22.
32. Corso SJ, Savoie FH, Geissler WB, Whipple TL, Jiminez W, Jenkins N. Arthroscopic repair of peripheral avulsions of the triangular fibrocartilage complex of the wrist: a multicenter study. Arthroscopy 1997;13:78-84.
33. Hauck RM, Skahen J 3rd, Palmer AK. Classification and treatment of ulnar styloid nonunion. J Hand Surg Am 1996;21:418-22.

 

34. Totterman SM, Miller RJ. MR imaging of the triangular fibrocartilage complex. Magn Reson Imaging Clin N Am 1995;3:213-28.
35. Amrami KK, Felmlee JP. 3-Tesla imaging of the wrist and hand: techniques and applications. Semin Musculoskelet Radiol 2008;12:223-37.
36. Mino DE, Palmer AK, Levinsohn EM. The role of radiography and computerized tomography in the diagnosis of subluxation and dislocation of the distal radioulnar joint. J Hand Surg Am 1983;8:23-31.
37. Cerezal L, del Piñal F, Abascal F, García-Valtuille R, Pereda T, Canga A. Imaging findings in ulnar-sided wrist impaction syndromes. Radiographics 2002;22:105-21.
38. Johnstone DJ, Thorogood S, Smith WH, Scott TD. A comparison of magnetic resonance imaging and arthroscopy in the investigation of chronic wrist pain. J Hand Surg Br 1997;22:714-8.
39. Oneson SR, Scales LM, Timins ME, Erickson SJ, Chamoy L. MR imaging interpretation of the Palmer classification of triangular fibrocartilage complex lesions. Radiographics 1996;16:97-106.
40. Lee YH, Choi YR, Kim S, Song HT, Suh JS. Intrinsic ligament and triangular fibrocartilage complex (TFCC) tears of the wrist: comparison of isovolumetric 3D-THRIVE sequence MR arthrography and conventional MR image at 3 T. Magn Reson Imaging 2013;31:221-6.
41. Schweitzer ME, Brahme SK, Hodler J, Hanker GJ, Lynch TP, Flannigan BD, Godzik CA, Resnick D. Chronic wrist pain: spin-echo and short tau inversion recovery MR imaging and conventional and MR arthrography. Radiology 1992;182:205-11. Erratum in: Radiology 1992;184:583.
42. Zanetti M, Bräm J, Hodler J. Triangular fibrocartilage and intercarpal ligaments of the wrist: does MR arthrography improve standard MRI? J Magn Reson Imaging 1997;7:590-4.
43. Scheck RJ, Romagnolo A, Hierner R, Pfluger T, Wilhelm K, Hahn K. The carpal ligaments in MR arthrography of the wrist: correlation with standard MRI and wristarthroscopy. J Magn Reson Imaging 1999;9:468-74.
44. Kirschenbaum D, Sieler S, Solonick D, Loeb DM, Cody RP. Arthrography of the wrist. Assessment of the integrity of the ligaments in young asymptomatic adults. J Bone Joint Surg Am 1995;77:1207-9.
45. Haims AH, Schweitzer ME, Morrison WB, Deely D, Lange RC, Osterman AL, Bednar JM, Taras JS, Culp RW. Internal derangement of the wrist: indirect MR arthrography versus unenhanced MR imaging. Radiology 2003;227:701-7.
46. Moser T, Khoury V, Harris PG, Bureau NJ, Cardinal E, Dosch JC. MDCT arthrography or MR arthrography for imaging the wrist joint? Semin Musculoskelet Radiol 2009;13:39-54.
47. Moser T, Dosch JC, Moussaoui A, Dietemann JL. Wrist ligament tears: evaluation of MRI and combined MDCT and MR arthrography. AJR Am J Roentgenol 2007;188:1278-86.
48. Lee RK, Griffith JF, Ng AW, Nung RC, Yeung DK. Wrist Traction During MR Arthrography Improves Detection of Triangular Fibrocartilage Complex and Intrinsic Ligament Tears and Visibility of Articular Cartilage. AJR Am J Roentgenol 2016;206:155-61.
49. Kang HS, Kindynis P, Brahme SK, Resnick D, Haghighi P, Haller J, Sartoris DJ. Triangular fibrocartilage and intercarpal ligaments of the wrist: MR imaging. Cadaveric study with gross pathologic and histologic correlation. Radiology 1991;181:401-4.
50. Steinbach LS, Smith DK. MRI of the wrist. Clin Imaging 2000;24:298-322.
51. Timins ME, Jahnke JP, Krah SF, Erickson SJ, Carrera GF. MR imaging of the major carpal stabilizing ligaments: normal anatomy and clinical examples. Radiographics 1995;15:575-87.
52. Burns JE, Tanaka T, Ueno T, Nakamura T, Yoshioka H. Pitfalls that may mimic injuries of the triangular fibrocartilage and proximal intrinsic wrist ligaments at MR imaging. Radiographics 2011;31:63-78.

**Cite this article as:** Ng AW, Griffith JF, Fung CS, Lee RK, Tong CS, Wong CW, Tse WL, Ho PC. MR imaging of the traumatic triangular fibrocartilaginous complex tear. Quant Imaging Med Surg 2017;7(4):443-460. doi: 10.21037/qims.2017.07.01

 